Evaluating Temporal and Spatial Variations in Vegetation Coverage in the Inner Mongolia Autonomous Region (2004-2023) Using *kNDVI*

Guangpu Wei[1¶], Wenjun Zhang[2¶], Zhiheng Zhu[1], Yaxian Gao[2], Xiaoyan Yu[2*]

Author information

School of Architecture and Art Design, Inner Mongolia University of Science and Technology, Baotou, Inner Mongolia, China

Guangpu Wei & Zhiheng Zhu

School of Economics and Management, Inner Mongolia University of Science and Technology, Baotou, Inner Mongolia, China

Wenjun Zhang, Yaxian Gao & Xiaoyan Yu

Research Center of Industrial Informationization and Innovation in Inner Mongolia University of Science and Technology, Baotou, Inner Mongolia, China

Wenjun Zhang, Yaxian Gao & Xiaoyan Yu

* Corresponding author

E-mail: yu_xiaoyan@imust.edu.cn

Abstract: The Inner Mongolia Autonomous Region (IMAR) is a crucial ecological zone in China, facing significant environmental challenges, particularly climate change. To better understand vegetation dynamics in this region, this study examines vegetation cover trends from 2004 to 2023 and identifies their driving factors using an innovative kernel-based Normalized Difference Vegetation Index (*kNDVI*) dataset from MOD13Q1 V6.1 data in Google Earth Engine (GEE). Spatiotemporal dynamics in vegetation cover were assessed using Theil-Sen median trend analysis, the Mann-Kendall test, and the Hurst exponent. Additionally, correlation analyses explored links between *kNDVI* and climate variables, including precipitation, temperature, and solar radiation (srad). Results revealed a northeast-to-west gradient in vegetation cover, with 35.36% of vegetation improving, 49.95% remaining stable, and 14.69% degrading. Future vegetation trends indicate 70.96% of the region has uncertain trajectories, while 29.04% shows potential for sustainable development. Among the climatic factors influencing vegetation cover, precipitation was the primary driver, followed by temperature and srad. Climatic factors were significant in western Hulunbuir and central Ulanqab, whereas non-climatic factors, including human activities and land-use changes, were dominant in Hulunbuir, Xing'an League, and Xilin Gol. These findings underscore the necessity for region-specific ecological management strategies integrating climatic and anthropogenic factors to enhance ecosystem resilience.

Keywords: spatiotemporal dynamics: vegetation cover: driving factors: ecological management: the IMAR

Vegetation coverage is a critical indicator for assessing ecosystem health and tracking change trends, and it has been widely applied in ecological monitoring and environmental assessment 1. The grassland ecosystems of the Inner Mongolia Autonomous Region (IMAR) function as a key ecological safeguard for China, with their growth directly affecting the stability and security of regional ecosystems 2. In recent years, intensified climate change and anthropogenic activities have resulted in significant spatio-temporal changes in the vegetation coverage across the IMAR 3. Most existing studies, however, rely on localized data analyses and traditional vegetation indices such as *NDVI*, which encounter challenges in the IMAR's arid and semi-arid environments including data gaps and spatial inconsistencies, limiting monitoring accuracy 45. Therefore, a more precise approach is urgently needed to address these challenges and enhance the accuracy and consistency of large-scale vegetation monitoring 6.

Although numerous studies highlight the impact of climatic variables and anthropogenic activities on vegetation dynamics, conventional vegetation indices face limitations in dry and semi-arid locations, thereby hindering their effectiveness for precise monitoring 78. To address these limitations, this research presents the kernel Normalized Difference Vegetation Index (*kNDVI*) as the primary vegetation monitoring index. By employing kernel-based interpolation, *kNDVI* achieves higher spatial continuity and consistency, enabling a more accurate reflection of the spatio-temporal changes in vegetation cover in the IMAR 910. Additionally, to evaluate long-term stability and trends in vegetation dynamics, the Hurst exponent is applied, which allows for the identification of persistence and self-sustainability in vegetation coverage. This comprehensive approach aids in predicting future vegetation trends and provides theoretical support for ecological management 111213.

This study uses MODIS remote sensing data from 2004 to 2023 to assess changes in vegetation coverage and its spatial distribution in the IMAR based on the *kNDVI*. The study seeks to quantify the impacts of climate factors and anthropogenic interventions on vegetation dynamics 1415. In addition to providing an innovative technical approach for vegetation monitoring, this study offers a scientific basis for formulating policies on ecological conservation and restoration 16. Through the integration of *kNDVI*, this research significantly enhances the accuracy of vegetation monitoring across large and complex ecological environments, demonstrating its significant potential and innovative value 1718.

1. Research Region

The Inner Mongolia Autonomous Region (IMAR) (37°24′–53°23′N, 97°12′–126°04′E), which is located in China's north, covers approximately 1.183 million square kilometers. It consists of seven distinct geomorphic units: the Alashan Plateau, Ordos Plateau, Inner Mongolian Plateau, Hulunbuir Plateau, Hetao Plain, Greater Khingan Mountains, and Northeast Plain 19. The region features a moderate continental monsoon climate, with temperatures and precipitation decreasing from northeast to west. Additionally, solar radiation (srad) decreases from west to northeast. The diverse vegetation types of this region are commonly referred to as "East Forest and West Mining, South Grain and North Pastoral" 20. The primary ecosystem types in the IMAR include grassland, woodland, desert, wetland, and sandy terrain, all of which play a crucial role in sustaining the local ecological equilibrium 21.

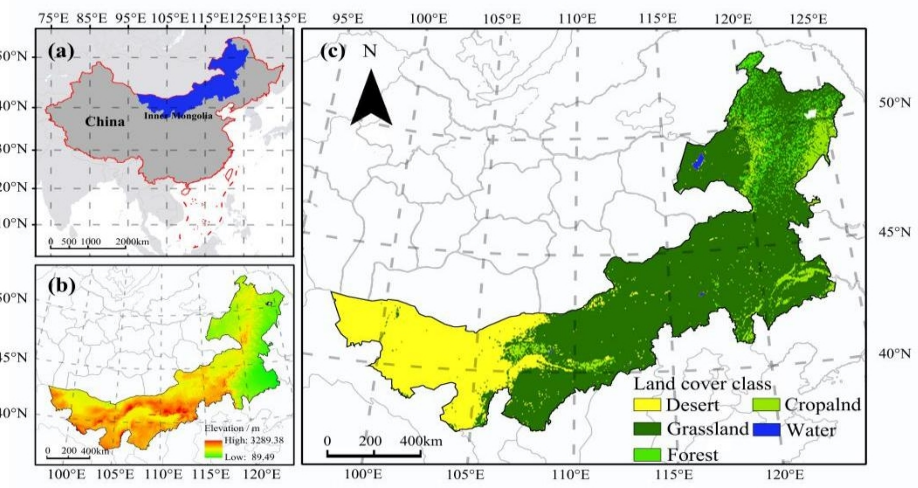

Figure 1. The study area (**a**) geographical position of the IMAR in China; (**b**) elevation distribution; (c) landscape types.

2. Methodology

2.1. Data Acquisition and Processing

The vegetation coverage data of the IMAR were gathered from the MOD13 Q1 V6.1 dataset (https://developers.google.com/). The data had a 250-meter of space resolution and were collected every 16 days. Annual *kNDVI* images from 2004 to 2023 were generated by computing *NDVI* data on a pixel-by-pixel basis using the GEE platform. The *kNDVI* calculation technique was utilized to evaluate vegetation dynamics over a 20-year span, providing significant insights into regional vegetation patterns and alterations. The *kNDVI* calculation formula is provided below:

$$\boldsymbol{kNDVI} = \tanh\left[\left(\frac{\mathbf{NIR} - \mathbf{red}}{2\sigma}\right)^2\right]$$

In the formula, the length scale parameter is designated for each unique application, indicating the index's sensitivity to sparse or thick vegetation areas; NIR refers to the near-infrared spectrum; Red denotes the red-light band; tanh represents the hyperbolic tangent function. An appropriate option is to calculate the mean:

$$kNDVI = \tanh\left(NDVI^2\right)$$

The temperature data employed in this investigation were obtained from the MOD11 A2 V6.1 average temperature dataset (https://developers.google.com). This dataset possesses a geographical resolution of 1,000 meters and updates at 8-day intervals. The precipitation and srad data were obtained from the IDAHO_EPSCOR/TERRACLIMATE dataset (https://developers.google.com), with a geographical resolution of 4.6 kilometers and a temporal resolution of 30 days. Utilizing the GEE platform (https://earthengine.google.com), we computed the average temperature, total precipitation, and mean srad from 2004 to 2023, and downloaded 20 images of temperature, precipitation, and srad for the same period. Additionally, the vector boundary data originated from the Resource and Environmental Science Data Platform (https://www.resdc.cn). The elevation data, which were obtained from the National Oceanic and Atmospheric Administration (https://www.ncei.noaa.gov), have a spatial resolution of 30 meters. Furthermore, land classification data were obtained from the Aerospace Information Innovation Research Institute under the Chinese Academy of Sciences (http://www.aircas.cn), featuring a spatial resolution of 30 meters. Before further analysis, all data were resampled to ensure consistency in both spatial and temporal resolutions.

2.2. Methods

The pattern of vegetation change was analyzed through Theil-Sen slope and the Mann-Kendall (MK) tests, using *kNDVI* and climatic data. To evaluate vegetation dynamics' sustainability in grasslands, the Hurst index was applied. When integrated with partial and complex correlation analysis methods, it provided valuable insights into vegetation responses to climate conditions and their key drivers (**Figure 2**).

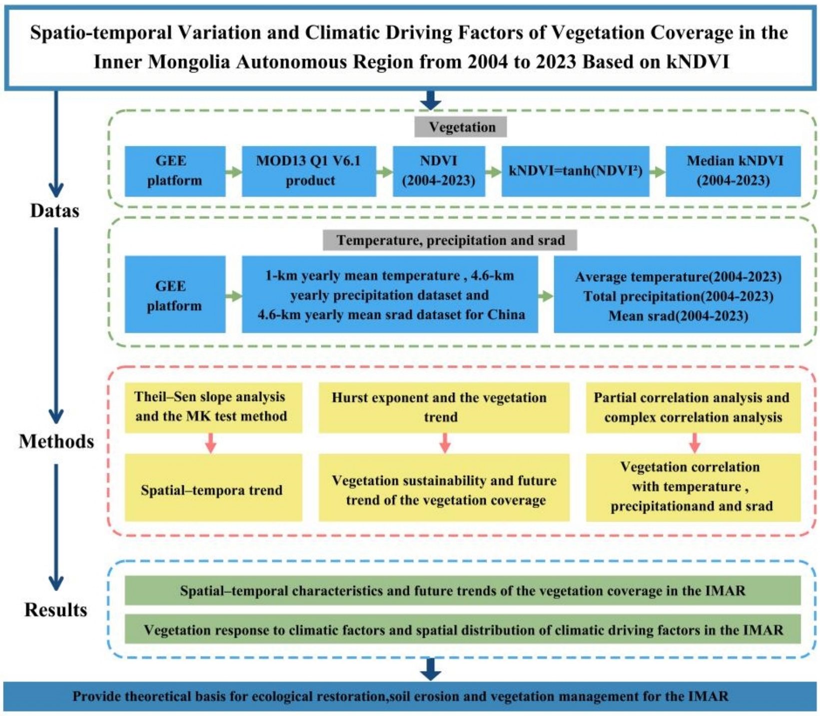

Figure 2. Workflow of the research process

2.2.1. Examination of Spatial-Temporal Dynamics and Future Forecasts

To analyze pixel-level vegetation trends over time, the Theil-Sen slope analysis and the MK test are often utilized in combination 222324. Theil-Sen slope analysis is recognized for its computational efficiency and robustness against measurement errors and discontinuous data 2526. Consequently, it was utilized to evaluate pixel-level *kNDVI* trends across the grasslands of IMAR from 2004 to 2023. Besides, to assess the statistical significance of vegetation trends, we employed the MK test, which is advantageous since it does not necessitate a certain distribution for the sample, reduces the impact of outliers, and does not require a stringent linear trend 2728. This testing methodology is extensively employed to assess the significance of patterns in longitudinal data sequences2930.

The integration of *kNDVI* trends with the Hurst exponent enables the forecasting of future vegetation trends 3132. This research divides the Hurst index value (H) into three categories: When H > 0.5, the *kNDVI* time series shows a trend consistent with its future trends; For H = 0.5, the *kNDVI* time series is classified as a random process lacking sustainability; when H < 0.5, it is considered unsustainable, suggesting a reverse trend in future *kNDVI* time series 3334. The formulas for S_{kNDVI} and Z_S are presented below:

$$S_{kNDVI} = \mathrm{Median}\left(\frac{kNDVI_j - kNDVI_i}{j-i}\right), 2004 \le i < j \le 2023 \qquad (3)$$

$$Z_s = \begin{cases} \dfrac{S-1}{\sqrt{var(S')}} & S > 0; \\ 0, & S = 0 \\ \dfrac{S+1}{\sqrt{var(S')}} & S < 0; \end{cases} \qquad (4)$$

$$\text{Where,} S = \sum_{i=1}^{n-1} \sum_{j=i+1}^{n} \mathrm{sgn}(x_j - x_i)$$

$$Var(S) = \frac{n(n-1)(2n+5) - \sum_{i=1}^{m} t_i(t_i-1)(2t_i+5)}{18}$$

S_{kNDVI} denotes the slope value calculated using the Theil-Sen method, and in the equations,

$kNDVI_i$ denotes the *kNDVI* value at pixel *i,* and $kNDVI_j$ denotes the value at pixel *j*; the Z_S parameter ranges from ($-\infty$ to $+\infty$); Z denotes the standardized test value; sgn indicates the sign function; n denotes the length of the *kNDVI* time series; m stands for the count of repeated datasets; and t_i denotes the number of repetitions within the interval. At a significance level α, if $|Z_S| > u_{1-\alpha/2}$, it implies substantial changes in the time series. In this investigation, we adopted the standard significance level of α = 0.05 to assess the pixel-level significance of *kNDVI* trends.

2.2.2. Analysis of Driving Factors

Partial correlation analysis was employed to investigate the relationships between *kNDVI* and climatic variables, including average temperature, total precipitation, and mean srad, in the IMAR from 2004 to 2023. The partial correlation coefficient (PCC) quantifies how strongly climatic factors influence vegetation. The significance of the PCC was then assessed with a *t*-test. Furthermore, we investigated the synergistic impacts of temperature, precipitation and srad on *kNDVI* through correlation analysis. Finally, to evaluate the association between *kNDVI* and the combined effects of temperature, precipitation, and srad, we computed the complex correlation coefficient (CCC) and assessed its significance using an F-test 3536.

Given the regional variations in the PCC and CCC between *kNDVI* and climatic variables, we utilized *t*-tests and F-tests to map and synthesize the spatial distribution of climatic driving factors affecting vegetation change in the IMAR. To ensure optimal consistency and regional continuity within each classification, the pixels satisfying the F-test criterion at a significance level of α = 0.05 were selected for further climate-driven spatial categorization, while those pixels not meeting this criterion were considered to be influenced by non-climatic factors. Utilizing the outcomes from comparing *kNDVI* with each climatic parameter, we classified the climatic driving factors into three distinct groups. The classification method is widely adopted as a determinant for vegetation cover 3738. The classification criteria are presented in Table 1.

Table 1. Criteria for classifying climatic driving forces influencing dynamic variations in *kNDVI*

Type of Driving Factor	Classification Basis			
	$R_{kNDVI-P}$	$R_{kNDVI-T}$	$R_{kNDVI-S}$	$R_{kNDVI-T-P-S}$
Driven by precipitation	$\lvert t\rvert>0.05$			$F>F_{0.05}$
Driven by temperature		$\lvert t\rvert>0.05$		$F>F_{0.05}$
Driven by srad			$\lvert t\rvert>0.05$	$F>F_{0.05}$
Driven by temperature, precipitation and srad	$\lvert t\rvert<0.05$	$\lvert t\rvert<0.05$	$\lvert t\rvert<0.05$	$F>F_{0.05}$
Driven by non-climate factors				$F<F_{0.05}$

Note: $R_{kNDVI-P}$, $R_{kNDVI-T}$ and $R_{kNDVI-S}$ represent the PCC between *kNDVI* and precipitation, temperature, and srad, respectively; $R_{kNDVI-P-T-S}$ denotes the CCC between *kNDVI* and the combined climatic variables (precipitation, temperature, and srad); $t_{0.05}$ indicates that the correlation is significant at the 0.05 level according to the *t*-test; $F_{0.05}$ signifies that the correlation is significant at the 0.05 level based on the F-test.

3. Result

3.1. Spatial and Temporal Characteristics of *kNDVI*

3.1.1. Spatial Patterns of Vegetation Coverage

The geographical distribution of the median *kNDVI* in the IMAR over the past two decades, based on *kNDVI* median data from 2004 to 2023, is depicted in **Figure 3**a. The spatial distribution of *kNDVI* in the IMAR, as shown in the figure, indicates significantly higher vegetation coverage in the northeast, diminishing towards the west. The mean *kNDVI* across the region was 0.109, with a variation range from 0 to 0.59. The mean *kNDVI* values for the western, central, and northeastern regions of the IMAR were 0.01, 0.05, and 0.26, respectively. Compared to the western region, the *kNDVI* values in the central and northeastern areas of the IMAR were higher. **Figure 3**b shows the statistical categorization outcomes of the median *kNDVI* and the distribution of each group throughout the 20-year period in the IMAR, utilizing the natural break point approach. The largest proportion of *kNDVI* values below 0.3 was seen in the IMAR, indicating limited vegetation coverage, mostly located in susceptible regions of the Alashan Plateau, Ordos Plateau, Hetao Plain, and the Inner Mongolian Plateau. Areas with *kNDVI* values between 0.03 and 0.07, representing median vegetation coverage, were predominantly located in southern Ulanqab, eastern Chifeng, the entirety of Tongliao, and western Hulunbuir. Areas with *kNDVI* values between 0.07 and 0.17 and those exceeding 0.17 were classified as having high and extremely high vegetation coverage, respectively. These regions primarily encompassed most of Hulunbuir, central Ulanqab, Xing'an League, Chifeng, and parts of Tongliao.

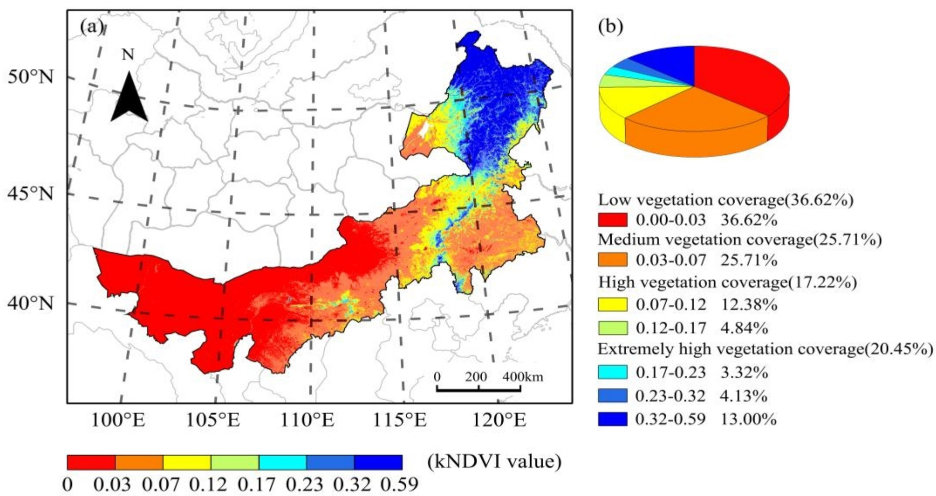

Figure 3. Geographical patterns and classification of vegetation cover: (**a**) median *kNDVI* from 2004 to 2023 in the IMAR (**b**) proportional distribution of each vegetation grouping

3.1.2. Temporal Dynamics of Vegetation Coverage

To investigate the temporal dynamics of *kNDVI* across the IMAR, annual median *kNDVI* values from 2004 to 2023 were employed to represent the overall vegetation condition for each year. **Figure** 4 displays a box plot summarizing the yearly distribution of *kNDVI* values, along with a line graph that illustrates the year-to-year fluctuations in median *kNDVI* throughout the study period. The *kNDVI* values in the IMAR exhibit a consistent trend with a variation rate of 0.011 every five years. The *kNDVI* values demonstrate significant fluctuations annually. The *kNDVI* values in the IMAR range from 0.089 to 0.133. The peak value was 0.133 in 2016, while the nadir was 0.089 in 2019.

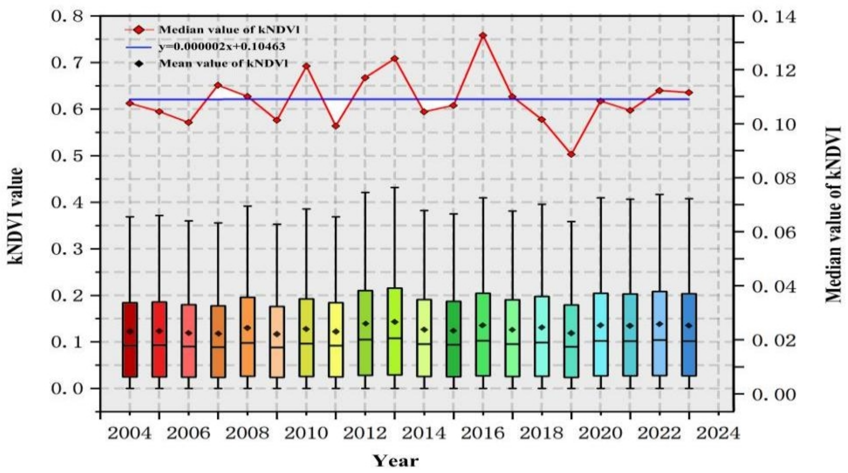

Figure 4. Annual variations of median *kNDVI* in IMAR (2004–2023). The box plots depict the annual distribution of *kNDVI* values (left axis), while the line graph shows the median *kNDVI* for each year (right axis).

3.1.3. Characteristics of Spatial Variation in Vegetation Coverage

The spatial patterns of *kNDVI* variation across the IMAR (2004–2023) were analyzed using Mann-Kendall tests and the Theil-Sen slope analysis. Since no pixels exhibited an S_{kNDVI} value of zero, we adapted classification methods from previous studies to develop our approach [39,40], resulting in the following classifications based on actual S_{kNDVI} conditions. We classified pixels into three categories based on their S_{kNDVI} values: stable vegetation areas (pixels with S_{kNDVI} values between -0.0005 and 0.0005), areas of vegetation increase (pixels with S_{kNDVI} values greater than or equal to 0.0005, $S_{kNDVI} \geq 0.0005$), and regions of vegetation degradation (pixels with S_{kNDVI} values less than or equal to -0.0005, $S_{kNDVI} \leq 0.0005$).

To determine the statistical significance of the *kNDVI* trends at each pixel, we applied the Mann-Kendall (MK) test using a confidence level of 0.05. A test result (Z_S) exceeding 1.96 or falling below -1.96 indicates a significant change. If $-1.96 < Z_S < 1.96$, the alteration is deemed negligible. By applying the Theil-Sen slope analysis in conjunction with the Mann-Kendall (MK) test, we mapped the pixel-level spatial distribution of annual *kNDVI* trends across the IMAR. As presented in Table 2, the results were classified into five distinct categories, and the proportion of region for each category was calculated accordingly. Regions showing increased vegetation coverage constituted 35.36% of the total, while those maintaining stable vegetation made up 49.95%. Conversely, regions with reduced vegetation coverage constituted 14.69%.

Table 2. Results of statistical study on *kNDVI* trends

S_{KNDVI}	Z_s Value	*kNDVI* Trends	Area Percentage/%
≥0.0005	≥1.96	Significantly improved	18.90
≥0.0005	-1.96-1.96	Slightly improved	16.46
-0.0005—0.0005	-1.96-1.96	Stable	49.95
≤-0.0005	-1.96-1.96	Slightly degraded	11.38
≤-0.0005	≦-1.96	Severely degraded	3.31

Note: Pixels with S_{KNDVI} values ranging from −0.0005 to 0.0005, and Z_S statistics satisfying $|Z_S| \geq 1.96$, were classified as stable vegetation regions.

Between 2004 and 2023 in the IMAR, the areas where vegetation coverage decreased were substantially more widespread than those where it increased, as shown in **Figure** 5. Regions with diminished vegetation coverage were predominantly situated in the eastern and western portions of Hulunbuir, Xing'an League, Tongliao, Chifeng, eastern Xilingol, southern Ulanqab, southeastern Ordos, southern Bayannur, and some parts in Hohhot and Baotou. The stable vegetation zones were mostly located in Alxa, northern Bayannur, northern Baotou, Ulanqab, western Xilingol, and western Hulunbuir. The region exhibiting an increase in vegetation coverage was limited, mostly in the middle and northern sectors of Hulunbuir, with minor extensions in Ulanqab, Chifeng, Xilingol, and Bayannur.

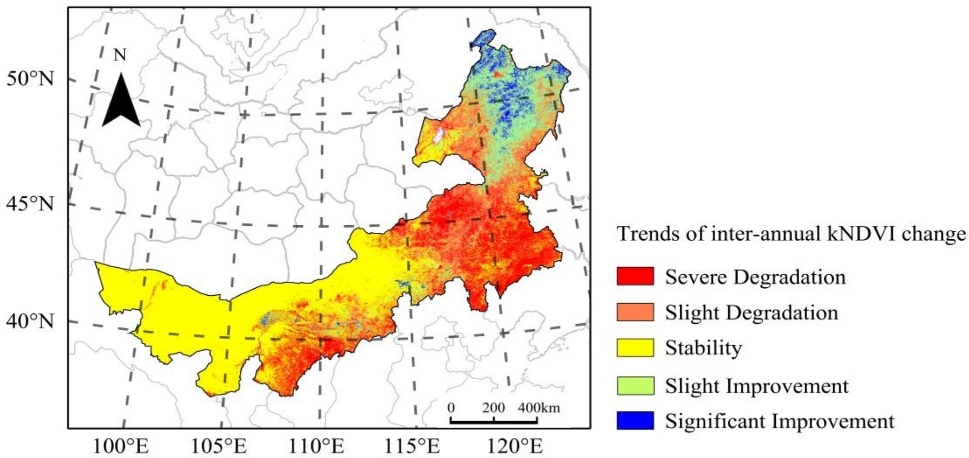

Figure 5. Annual variations of *kNDVI* in the IMAR from 2004 to 2023

3.1.4. Emerging patterns of Vegetation Coverage in the IMAR

In the IMAR, the average H value of *kNDVI* was determined to be 0.371, with 75.7% of the regions exhibiting H values below 0.5, as shown in Figure 6a. This suggests that vegetation coverage changes in most regions follow a periodic or gradually declining trend, with a degree of negative long-term memory. Conversely, 24.3% of the regions exhibited H values exceeding 0.5, indicating that in these areas, the trends in vegetation coverage were more persistent and demonstrated favorable long-term memory. This suggests significant durability of the *kNDVI* in the IMAR. To clarify the heterogeneity of vegetation trends and their sustainability, we combined the shifting trends of *kNDVI* with the corresponding H values. This approach enabled us to extract coupling information between trend dynamics and sustainability. As presented in **Figure 6**b, six distinct scenarios derived from the coupling results. Notably, regions with H values below 0.5 from 2004 to 2023, regardless of the nature of *kNDVI* trends, were classified as having uncertain future trends.

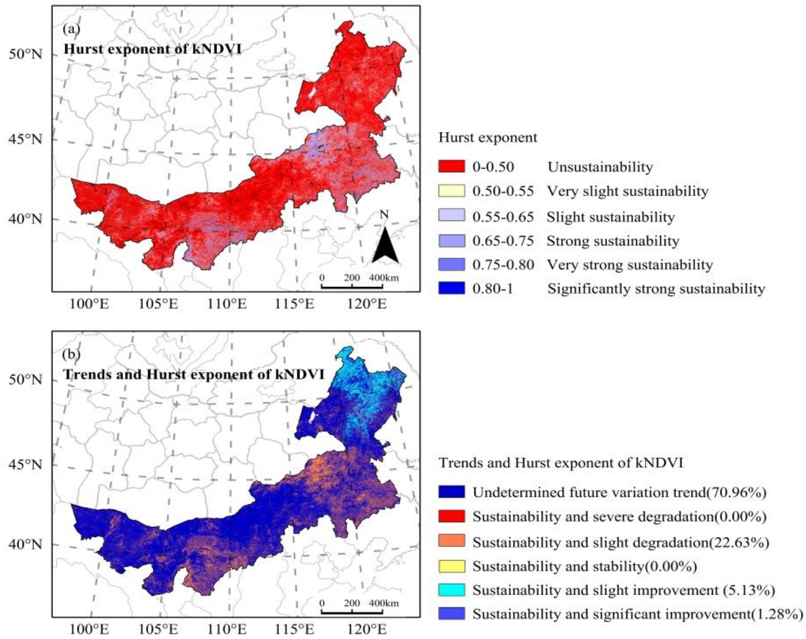

Figure 6. Patterns of the Hurst exponent and projected vegetation dynamics: (a) map depicting the variation of the Hurst exponent across the region (b) map illustrating the anticipated future trends of *kNDVI*, based on current *kNDVI* changes and their sustainability.

As illustrated in **Figure 6**b, the IMAR displays varied regional distributions of projected *kNDVI* trends. Areas classified as exhibiting "sustainability and improvement" comprised 6.41% of the total region, predominantly situated in the central and northern parts of Hulunbuir, with a smaller fraction extending into Xing'an League. The ratio of regions designated as "sustained stability" and "sustained severe degradation" was 0.22. Nevertheless, 63% of the overall region showed "sustained and slight degradation". These areas were chiefly distributed across the Northeast Plain, the southern reaches of the Greater Khingan Range, the eastern sector of Inner Mongolia's plateau, the Hetao Plain, and the Ordos Plateau, with a minor extension into the Alashan Plateau. Regions with uncertain future trends constituted 70.96%, predominantly located in the western and eastern sectors of Hulunbuir, Xilingol, Bayannur, and Alxa.

3.2. Factors Influencing Vegetation Coverage

3.2.1. Spatiotemporal Dynamics Patterns of Climatic Factors

Temporal variations in climatic variables across the IMAR from 2004 to 2023 were examined by extracting pixel-level data on temperature, precipitation, and srad from images representing the average temperature, total precipitation, and mean srad. Leveraging these datasets, we characterized the general climatic patterns on a yearly basis. The analysis of the average temperature, precipitation, and srad data from 2004 to 2023 illustrates the regional distribution characteristics of the IMAR's climate. **Figures** 7a–c revealed that temperature, precipitation, and srad throughout IMAR had generally exhibited upward trends with fluctuations. These findings are crucial for restoring ecosystems and promoting sustainable progress within the IMAR. In the IMAR, the annual average temperature increased by approximately 0.3 °C/5a, total annual precipitation by 27 mm/5a, and the annual mean srad by 0.525 W/m². Consequently, the climate in the IMAR demonstrated a clear pattern of rising temperature and humidity. To reveal the spatial patterns of temperature, precipitation, and srad, we applied a statistical classification method to divide these variables into ten distinct categories. **Figures 7d–f** illustrate that from 2004 to 2023, the IMAR had an average temperature of 16.36°C, total average precipitation of 274.1 mm, and mean srad of 180.03 W/m². The temperature exhibited geographic variation, fluctuating between -3.1°C and 36.44°C from northeast to west. Precipitation varied from 27 to 556 mm, with an increase from the west to the northeast. The srad steadily decreased from west to northeast, ranging from 139.46 to 199.27 W/m². Moreover, there was significant geographical diversity in temperature, precipitation, and srad across the IMAR.

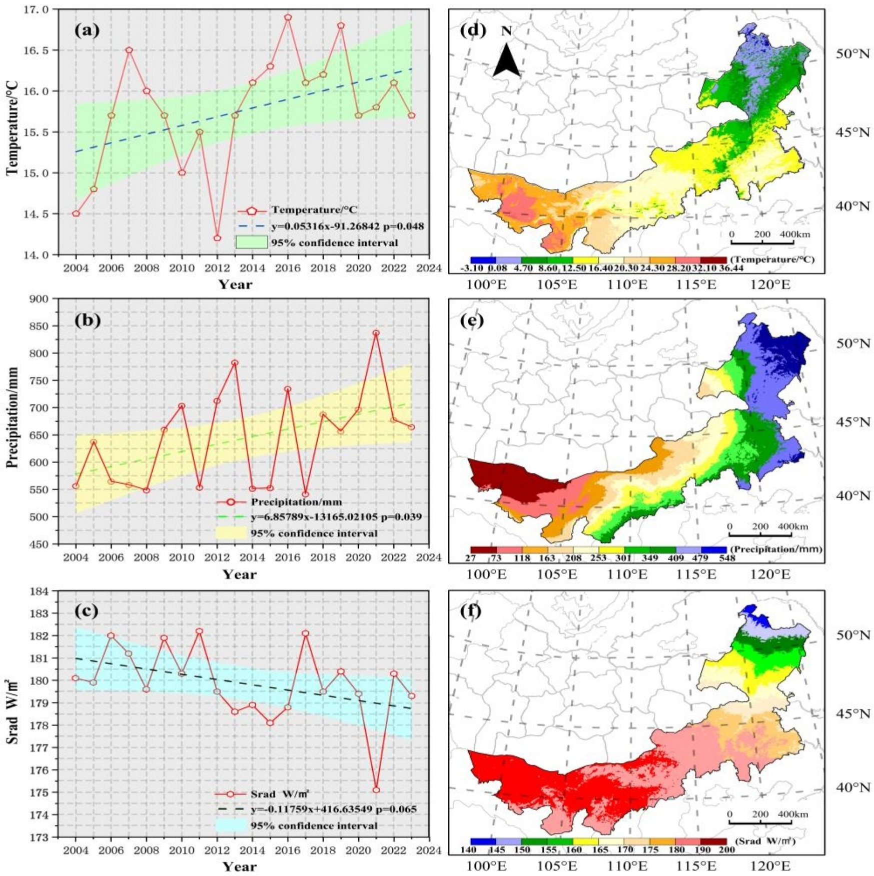

Figure 7. Temporal trends and spatial distributions of climatic variables in IMAR (2004–2023): (**a**) temporal variations in average temperature (**b**) temporal variations in total precipitation (**c**) temporal variations in mean srad (**d**) spatial patterns of average temperature distribution (**e**) spatial patterns of total precipitation distribution (**f**) spatial patterns of mean srad distribution.

3.2.2. Analysis of Partial Correlations Between *kNDVI* and Climatic Variables

Employing the breakpoint method, we classified the regional patterns of partial correlation coefficients (PCC) between *kNDVI* and climatic factors. Between 2004 and 2023, the PCC relating *kNDVI* to temperature ranged from -1 to 1, with an average of -0.11 (**Figure 8**a). Pixels exhibiting positive correlation (56.33%) were more prevalent than those demonstrating negative correlation (43.67%), with 31.77% categorized as "significantly positively correlated" and 22.31% as "significantly negatively correlated" (**Figure 8**b). The results demonstrated significant variation in the regional distribution pattern of PCC across *kNDVI* and temperature. The pixels with a strong positive correlation were predominantly located in central Xilingol, southern Chifeng and Tongliao, western Ordos, and eastern Alxa. In contrast, negatively correlated pixels were predominantly located in the northeast and south of Hulunbuir, throughout most of Xing'an League, northern Tongliao, Ulanqab, southern Hohhot, the majority of Bayannur, southern Ordos, and western and southern Alxa League. Pixels with significant negative correlation were primarily observed in Hulunbuir, Xing'an League, Xilingol, Hohhot, and Ordos.

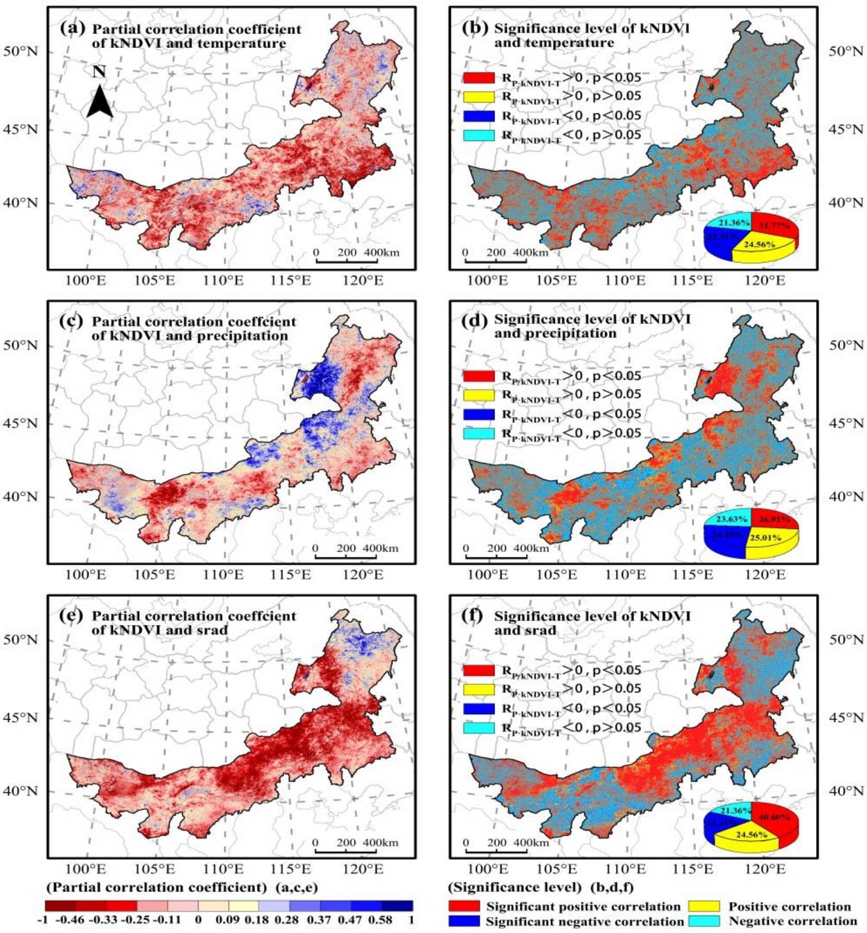

Figure 8. Spatial analysis of PCC and significance levels between *kNDVI* and climatic factors: **(a)** PCC between *kNDVI* and temperature, ($R_{kNDVI-T}$) **(b)** significance level corresponding to $R_{kNDVI-T}$ **(c)** PCC between *kNDVI* and precipitation,($R_{kNDVI-P}$) **(d)** significance level corresponding to $R_{kNDVI-P}$ **(e)** PCC between *kNDVI* and srad,($R_{kNDVI-S}$) **(f)** significance level corresponding to $R_{kNDVI-S}$

From 2004 to 2023, the PCC between *kNDVI* and precipitation spanned the entire range from -1 to 1, averaging 0.02 (**Figure 8**c). Pixels with positive correlation constituted 51.92%, whilst those with negative correlation comprised 48.08%. **Figure 8**d demonstrates that the pixels with a strong positive correlation were primarily situated in the western region of Hulunbuir, the eastern region of Xilingol, the central region of Ulanqab, and along the boundary between Alxa and Bayannur. The pixels exhibiting significant negative correlation and negative correlation were predominantly distributed across eastern and northern regions of Hulunbuir, Xing'an League, Chifeng, Tongliao, central Xilingol, northern Ulanqab, Baotou, Hohhot, the majority of Ordos, eastern and northern Bayannur, and most of Alxa.

The PCC between *kNDVI* and srad spanned the entire possible range, with an average of -0.18 (**Figure 8**e). Positive correlations were observed in 65.16% of the pixels, surpassing the 34.84% that showed negative correlations. **Figure 8**f demonstrates that significant positive correlations were primarily identified in western Hulunbuir, eastern Xilingol, central Ulanqab, and along the boundary between Bayannur and Alxa. Significant negative and negative correlations were predominantly observed in eastern and northern Hulunbuir, Xing'an League, Chifeng, Tongliao, central and western Xilingol, northern Ulanqab, Baotou, Hohhot, most of Ordos, northern Bayannur, and much of Alxa. The vegetation in the IMAR exhibited a pronounced sensitivity to climatic conditions, ranked in influence as follows: precipitation, temperature, and srad.

3.2.3. Examination of Determinants Influencing Vegetation Coverage

Applying the breakpoint method, we categorized the cross-correlations between *kNDVI* and climatic variables, as depicted in **Figure 9**a, with their significance levels shown in **Figure 9**b. Within the IMAR, these correlations exhibited a broad range and averaged 0.44. Notably, only 32.5% of the pixels demonstrated statistically significant correlations at the 0.05 level.

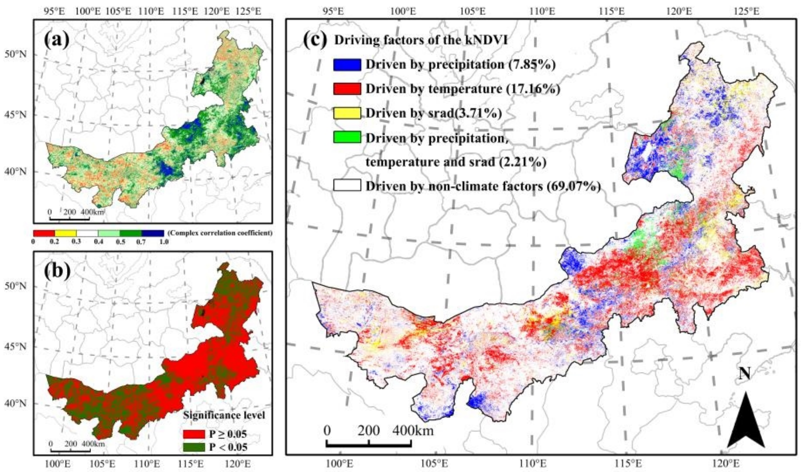

Figure 9. Determinants of *kNDVI* Analysis: (**a**) regional distribution of the CCC between *kNDVI* and climatic variables (**b**) significance levels of the CCC (**c**) factors influencing *kNDVI* in the IMAR (2004-2023)

Analyzing correlations from 2004 to 2023 revealed spatiotemporal variability within the IMAR. The vegetation patterns, influenced by climatic conditions, were categorized into distinct zones. **Figure 9**c depicts the regional distribution of these driving forces. The findings revealed that only 30.93% of the vegetation coverage in the IMAR was influenced by climatic variables, whereas 69.07% was influenced by non-climatic factors. Climatic factors, specifically precipitation, influenced 7.85% of the regions, predominantly in Hulunbuir, western Xilingol, southern Ulanqab, southwestern Ordos, and southern Alxa. The temperature-driven zone covered 17.16% of the area, primarily situated in the eastern region of Alxa and the northern sections of Ordos, Baotou City, Ulanqab, Xilingol, Chifeng, southern Tongliao, Xing’an League, and both eastern and western parts of Hulunbuir. The srad-driven area constituted 3.71%, ~~was~~ primarily distributed in northern Hulunbuir, eastern Xing’an League, and central Ulanqab, Baotou City, and Alxa. The region affected by temperature, precipitation, and srad accounted for 2.21% of the total, predominantly located in the western half of Hulunbuir, the western section of Xing’an League, and the central-eastern zone of Xilingol. Our findings suggest that in the IMAR, vegetation was predominantly influenced by non-climatic factors, and this influence was observed across many cities throughout the region.

4. Discussion

4.1. Temporal Evolution and Spatial Distribution of *kNDVI*

From 2004 to 2023, we investigated the temporal and spatial variations of *kNDVI* across the IMAR. The analysis revealed that vegetation coverage was notably higher in the northeastern region (**Figure 3**a), likely due to humid climatic conditions, ample precipitation, and the presence of wetland ecosystems 4142. The predominant plant type was grassland, with the exception of trees and bushes. By contrast, the biological habitat in the western region, which was predominantly influenced by environmental variables 43 was more fragile, as indicated by the low *kNDVI* values. This fragility was particularly evident in areas such as Alxa. Alxa hosts the expansive Badain Jaran Desert, covering approximately 49,000 square kilometers and recognized as one of China’s largest deserts. Similarly, the Tengger Desert in Alxa Left Banner extends over 43,000 square kilometers, ranking among the country’s most extensive desert regions. Additionally, the Kubuqi Desert and Ulanbuhe Desert, which cover smaller area, are situated to the west of the IMAR 44.

In comparison to other research, vegetation coverage data exhibited a consistent and declining trend overall (**Figure 4**). The "stable" vegetation coverage category was the predominant one in the IMAR, although the "uncertain future trend" category also represented a significant portion (**Figure 5** and **Figure 6**b). The prevalence may be attributed to the influence of various factors on surface vegetation changes, such as climate change, alterations in land use, and human activities, with their interactions potentially being complex, resulting in uncertainty about future trends 4546.

Nonetheless, the percentage of "sustainable and slightly degraded" regions was also notably high, indicating "very strong sustainability", which implies that vegetation coverage in the IMAR has likely experienced a minor decline in the recent past and may continue to decline in the foreseeable future. This is mostly due to natural factors, human activities, or other environmental causes that negatively impact vegetation in these areas 47. Agriculture and animal husbandry have consistently been foundational sectors in the IMAR, and overgrazing has caused grassland degradation, leading to a notable reduction in vegetation cover. However, certain areas have exhibited "sustainability and substantial enhancement". This favorable advancement may be chiefly ascribed to the government's implementation of various ecological protection laws aimed at increasing vegetation coverage and restoring the ecological environment. The government has strengthened the protection of vegetative resources, including grasslands and forests, imposed restrictions on development and logging, and implemented policies to convert cropland into forests and grasslands 4849. Nevertheless, there has been a slight reduction in the overall vegetation across the IMAR.

4.2. Analysis of the Influencing Factors on *kNDVI*

The analysis revealed that non-climatic factors significantly influence vegetation in the IMAR

(**Figure 9**c), indicating that key drivers of *kNDVI* differ across regions 50. Prior studies have identified anthropogenic activities, precipitation, temperature, and srad as the principal determinants of vegetation coverage 51. In areas with minimal human impact, fluctuations in vegetation coverage were primarily attributed to weather influences 52.

The investigation into the regional distribution of driving forces indicated notable spatial variability in climatic variables throughout the IMAR. Most precipitation-dependent regions were located in dry or semi-arid zones, where rainfall is often limited. Conversely, areas affected by temperature tended to experience relatively low temperatures. Regions impacted by strong srad were predominantly located in low-latitude zones with sparse vegetation, particularly those below 500 meters in elevation. Conversely, regions affected by a confluence of precipitation, temperature, and srad were predominantly situated at elevated heights, especially in Xilingol, where the elevation surpasses 1,000 meters. Geographical variations highlight the influence of height and topography on climatic elements including temperature, moisture availability, and light, which directly impact plant distribution 53. Therefore, areas which are susceptible to natural disasters should use tailored strategies to improve resilience to cold and drought, based on their specific climate conditions.

Incorporating precipitation, temperature, and srad into vegetation management establishes a robust foundation for enhancing plant development and sustaining ecological equilibrium. Effective measures include careful consideration of local climatic and hydrological conditions to prevent problems such as overplanting and excessive soil moisture loss. Customized and knowledgeable strategies are essential for achieving sustainable vegetation management 54.

4.3. Limitations and Guidelines for Subsequent Research

This study analyses trends in vegetation change, assesses the long-term stability of vegetation dynamics, and it also examines the influence of climatic factors on the spatial distribution of vegetation in the IMAR. The findings of this study can facilitate the efficient monitoring of vegetation alterations and provide a theoretical foundation for conservation and rehabilitation initiatives in the IMAR.

Nevertheless, our study has several limitations. Firstly, although prospective vegetation changes can be quantified by integrating *kNDVI* trends and H values, the Hurst index fails to offer insights into the longevity of sustainable vegetation dynamics. Therefore, it is essential to develop methodologies that can more accurately capture temporal patterns 55. Additionally, in some years, the yearly median *kNDVI* values were very low, which allowed for the identification of interference years and regions of vegetation coverage from 2004 to 2023. This limitation calls for further examination of the factors affecting plant growth. Temperature, precipitation, and srad were identified as major climate-related elements influencing vegetation coverage, yet the complex interplay between these factors and topography at micro and macro scales could not be fully captured 56. Lastly, several natural factors, such as soil composition and runoff, also affect vegetation coverage, suggesting a need for more comprehensive data in future studies. Consequently, further research should examine these natural factors that were not addressed in this study 57.

Moreover, non-climatic factors exert a significant influence on vegetation coverage in the IMAR. Over time, the complexity of vegetation dynamics has been substantially affected by anthropogenic activities such as urban expansion, infrastructure development, grazing, and changes in land use and land cover (LUCC). Therefore, future research should focus on integrating these anthropogenic variables into studies to better understand their geographical effects on vegetation 58.

5. Conclusions

In this study, calculations of *kNDVI* were performed on the GEE platform using MOD13Q1 V6.1 data. The annual median *kNDVI* values from 2004 through 2023 were utilized as indicators of vegetation status for each respective year. We analyzed the spatiotemporal characteristics of *kNDVI* across the IMAR by correlating it with temporal datasets of temperature, precipitation, and srad. This approach revealed *kNDVI*'s sensitivity to climatic variables and other driving forces.

The findings indicated that vegetation coverage in the IMAR was substantially higher in northeastern regions and decreased towards the west, exhibiting considerable spatial variability. Specifically, the yearly median *kNDVI* varied between 0.089 and 0.133 from 2004 to 2023, indicating a consistent trend. Over this period, 35.36% of vegetation coverage in the IMAR showed improvement, 49.95% remained stable, and 14.69% experienced degradation. In terms of sustainability, 70.96% of the vegetation coverage exhibited "unpredictable future trends", while 29.04% was classified as sustainable, including 6.41% categorized as "sustainability and improvement" and 22.63% as "sustainability and degradation". Furthermore, vegetation coverage was strongly influenced by climatic factors, ranked in order of influence as follows: precipitation, temperature, and srad. At a 0.05 confidence level, non-climatic factors influenced 69.07% of the vegetation, predominantly across much of Hulunbuir, Xing'an League, Ulanqab, Baotou, Hohhot, Bayannur, Wuhai, and extensive areas of Alxa. In contrast, 30.93% of vegetation changes were driven by climatic factors, mainly in the western Hulunbuir and Xing'an League, Xilingol, central

Ulanqab, central Baotou, and eastern Alxa. Overall, this study integrates *kNDVI* with various analytical methods to offer a robust approach for monitoring vegetation dynamics in large-scale, ecologically complex environments. The findings provide valuable scientific insights to support ecological restoration and sustainable development efforts in the IMAR.

Author Contributions:

† These authors contributed equally to this work.

Investigation, Methodology, and Analysis: G.W. and W.Z.; Supervision and Validation: X.Y. and Z.Z.; Writing—Original Draft: W.Z.; Writing—Review and Editing: G.W. and Y.G. All authors read and approved the final manuscript.

Funding:

Natural Science Foundation of Inner Mongolia Autonomous Region (2022LHMS07004).

Ethical standards

The experiments comply with the current laws of the country in which they were performed.

Data Availability Statement:

The data presented in this study can be obtained by contacting the corresponding author upon request.

Conflicts of Interest:

The authors declare no conflicts of interest.

References

1. De Carvalho RM, Szlafsztein CF. Urban vegetation loss and ecosystem services: The influence on climate regulation and noise and air pollution. *Environmental Pollution.* 2019, 245, 844-852.

2. Li S, Xie YC, Brown DG, Bai YF, Hua J, Judd K. Spatial variability of the adaptation of grassland vegetation to climatic change in Inner Mongolia of China. *Applied Geography.* 2013, 43, 1-12.
3. Li JZ, Liu YM, Cao MM, Xue B. Space-Time Characteristics of Vegetation Cover and Distribution: Case of the Henan Province in China. *Sustainability.* 2015, 7, 11967-11979.
4. Hu MM, Xia BC. A significant increase in the normalized difference vegetation index during the rapid economic development in the Pearl River Delta of China. *Land Degradation & Development.* 2019*,* 30*,* 359-370.
5. Gui X, Wang LC, Yao R, Yu DQ, Li CA. Investigating the urbanization process and its impact on vegetation change and urban heat island in Wuhan, China. *Environmental Science and Pollution Research.* 2019, 26,30808-30825.
6. Propastin PA. 2009 Spatial non-stationarity and scale-dependency of prediction accuracy in the remote estimation of LAI over a tropical rainforest in Sulawesi, Indonesia. *Remote Sensing of Environment.* 2009, 113, 2234-2242.
7. Guerschman JP, Hill MJ, Renzullo LJ, Barrett DJ, Marks AS, Botha EJ. Estimating fractional cover of photosynthetic vegetation, non-photosynthetic vegetation and bare soil in the Australian tropical savanna region upscaling the EO-1 Hyperion and MODIS sensors. *Remote Sensing of Environment.* 2009, 113, 928-945.
8. Jjagwe P, Chandel AK, Langston D. Pre-Harvest Corn Grain Moisture Estimation Using Aerial Multispectral Imagery and Machine Learning Techniques. Land. 2023, 12, 2188.
9. Gu Z, Chen X, Ruan W, Zheng M, Gen K, Li X, Deng H, Chen Y, Liu M. Quantifying the direct and indirect effects of terrain, climate and human activity on the spatial pattern of *kNDVI*-based vegetation growth: A case

study from the Minjiang River Basin, Southeast China. *Ecological Informatics*. 2024, 80, 102493.

10. Yu H, Yang Q, Jiang S, Zhan B, Zhan C. Detection and Attribution of Vegetation Dynamics in the Yellow River Basin Based on Long-Term Kernel *NDVI* Data. *Remote Sensing*. 2024, 16, 1280.

11. Peng J, Liu Z, Liu Y, Wu J, Han Y. Trend analysis of vegetation dynamics in Qinghai–Tibet Plateau using Hurst Exponent. *Ecological Indicators*. 2012, 14, 28-39.

12. Wang J, Zhao J, Zhou P, Li K, Cao Z, Zhang H, Han Y, Luo Y, Yuan X. Study on the spatial and temporal evolution of NDVI and Its Driving Mechanism Based on Geodetector and Hurst Indexes: a case study of the Tibet Autonomous Region. *Sustainability*. 2023, 15, 5981.

13. Tran TV, Tran DX, Nguyen H, Latorre Carmona P, Myint SW. Characterising spatiotemporal vegetation variations using LANDSAT time - series and Hurst exponent index in the Mekong River Delta. *Land Degradation & Development*. 2021, 32, 3507-3523.

14. Li A, Wu J, Huang J. Distinguishing between human-induced and climate-driven vegetation changes: a critical application of RESTREND in inner Mongolia. *Landscape ecology*. 2012, 27, 969-982.

15. Zhu L, Shi M, Fan D, Tu K, Sun W. Analysis of changes in vegetation carbon storage and net primary productivity as influenced by land-cover change in inner Mongolia, China. *Sustainability*. 2023, 15, 4735.

16. Tian H, Cao C, Chen W, Bao S, Yang B. Myneni RB. Response of vegetation activity dynamic to climatic change and ecological restoration programs in Inner Mongolia from 2000 to 2012. *Ecological Engineering*. 2015, 82, 276-289.

17. Guo B, Zhang R, Lu M, Xu M, Liu P, Wang L. A New Large-Scale Monitoring Index of Desertification Based on Kernel Normalized Difference Vegetation Index and Feature Space Model. *Remote Sensing*. 2024, 16, 1771.

18. Wang Q, Moreno-Martínez Á, Muñoz-Marí J, Campos-Taberner M, Camps-Valls G. Estimation of vegetation

traits with kernel NDVI. *ISPRS Journal of Photogrammetry and Remote Sensing*. 2023, 195, 408-417.

19. Nanzad L, Zhang J, Tuvdendorj B, Yang S, Rinzin S, Prodhan FA, Sharma TP. Assessment of drought impact on net primary productivity in the terrestrial ecosystems of Mongolia from 2003 to 2018. *Remote Sensing*. 2021, 13, 2522.
20. Fang J, Piao S, Tang Z, Peng C, Ji W. Interannual variability in net primary production and precipitation. *Science*. 2001, 293, 1723.
21. Qi J, John R, Groisman P, Chen J. Understanding livestock production and sustainability of grassland ecosystems in the Asian Dryland Belt. *Ecological Processes*. 2017, 6, 1-10.
22. Yeh HF, Yeh CF, Lee CH. Mann-Kendall test and Theil-Sen estimator for long-term spatial and temporal trends of streamflow in Taiwan. *Journal of Chinese Soil and Water Conservation*. 2016, 47, 73-83.
23. Fensholt R, Proud SR. Evaluation of Earth Observation based global long term vegetation trends—Comparing GIMMS and MODIS global NDVI time series. *Remote sensing of Environment*. 2012, 119, 131-147.
24. Li P, Wang J, Liu M, Xue Z, Bagherzadeh A, Liu M. Spatio-temporal variation characteristics of *NDVI* and its response to climate on the Loess Plateau from 1985 to 2015. *Catena*. 2021, 203, 105331.
25. Xu T, Wu H. Spatiotemporal analysis of vegetation cover in relation to its driving forces in Qinghai–Tibet Plateau. *Forests*. 2023, 14,1835.
26. Ay M, Kisi O. Investigation of trend analysis of monthly total precipitation by an innovative method. *Theoretical and Applied Climatology*. 2015, 120, 617-629.
27. Bao G, Qin Z, Bao Y, Zhou Y, Li W, Sanjjav A. NDVI-based long-term vegetation dynamics and its response to climatic change in the Mongolian Plateau. *Remote Sensing*. 2014, 6, 8337-8358.
28. AlSubih M, Kumari M, Mallick J, Ramakrishnan R, Islam S, Singh CK. Time series trend analysis of rainfall

in last five decades and its quantification in Aseer Region of Saudi Arabia. *Arabian Journal of Geosciences*. 2021, 14, 1-5.

29. Neeti N, Eastman JR. A contextual mann-kendall approach for the assessment of trend significance in image time series. *Transactions in GIS*. 2011, 15, 599-611.
30. Güçlü YS. 2018 Multiple Şen-innovative trend analyses and partial Mann-Kendall test. *Journal of Hydrology*. 2018, 566, 685-704.
31. Zhao JP, Guo EL, Wang YF, Kang Y, Gu XL. Ecological drought monitoring of Inner Mongolia vegetation growing season based on kernel temperature vegetation drought index (*kTVDI*). *Ying Yong Sheng tai xue bao= The Journal of Applied Ecology*. 2023, 34, 2929-2937.
32. Chen Z, Zhang X, Jiao Y, Cheng Y, Zhu Z, Wang S, Zhang H. Investigating the spatio-temporal pattern evolution characteristics of vegetation change in Shendong coal mining area based on *kNDVI* and intensity analysis. *Frontiers in Ecology and Evolution.* 2023, 11, 1344664
33. Qiao X, Zhang J, Liu L, Zhang J, Zhao T. Spatiotemporal Changes in Vegetation Cover during the Growing Season and Its Implications for Chinese Grain for Green Program in the Luo River Basin. *Forests.* 2024, 15, 1649.
34. Kang Y, Guo E, Wang Y, Bao Y, Bao Y, Mandula N. Monitoring vegetation change and its potential drivers in Inner Mongolia from 2000 to 2019. *Remote Sensing*. 2021, 13, 3357.
35. Piao S, Fang J, Zhou L, Ciais P, Zhu B. Variations in satellite‐derived phenology in China's temperate vegetation. *Global change biology*. 2006, 12, 672-685.
36. Gao N, Zhou J, Zhang X, Cai W, Guan T, Jiang L, Du H, Yang D, Cong Z, Zheng Y. 2017 Correlation between vegetation and environment at different levels in an arid, mountainous region of China. *Ecology and Evolution*.

2017, 7, 5482-5492.

37. Behjat V, Mahvi M, Rahimpour E. New statistical approach to interpret power transformer frequency response analysis: non-parametric statistical methods. *IET Science, Measurement & Technology*. 2016, 10, 364-369.

38. Feng X, Tian J, Wang Y, Wu J, Liu J, Ya Q, Li Z. Spatio-temporal variation and climatic driving factors of vegetation coverage in the Yellow River Basin from 2001 to 2020 based on *kNDVI*. *Forests*. 2023, 14, 620.

39. Ahmed SM. Assessment of irrigation system sustainability using the Theil–Sen estimator of slope of time series. *Sustainability science.* 2014, 9, 293-302.

40. Some’e BS, Ezani A, Tabari H. Spatiotemporal trends and change point of precipitation in Iran. *Atmospheric research.* 2012, 113, 1-2.

41. Piao S, Fang J, Ciais P, Peylin P, Huang Y, Sitch S, Wang T. The carbon balance of terrestrial ecosystems in China. *Nature.* 2009, *458*, 1009-1013.

42. Zhang X, Hu Y, Zhuang D, Qi Y, Ma X. *NDVI* spatial pattern and its differentiation on the Mongolian Plateau. Journal of geographical sciences. 2009, 19, 403-415.

43. Li D, Liu K, Wang S, Wu T, Li H, Bo Y, Zhang H, Huang Y, Li X. Four decades of hydrological response to vegetation dynamics and anthropogenic factors in the Three-North Region of China and Mongolia. *Science of The Total Environment*. 2023, 857, 159546.

44. Wang M, Dong Z, Luo W, Lu J, Li J. Spatial variability of vegetation characteristics, soil properties and their relationships in and around China’s Badain Jaran Desert. *Environmental Earth Sciences.* 2015, 74, 6847-6858.

45. Zhang Y, Wang Q, Wang Z, Yang Y, Li J. Impact of human activities and climate change on the grassland dynamics under different regime policies in the Mongolian Plateau. *Science of the Total Environment.* 2020, 698, 134304.

46. He D, Huang X, Tian Q, Zhang Z. Changes in vegetation growth dynamics and relations with climate in inner Mongolia under more strict multiple pre-processing (2000–2018). *Sustainability.* 2020, 12, 2534.

47. Kuan CH, Chenchen YA, Liga BA, Yu CH. Rui LI, Luomeng, C.H. Effects of natural and human factor on vegetation normalized difference vegetation index based on geographical detectors in Inner Mongolia. *Acta Ecologica Sinica*. 2021, 12,1-3.

48. Li W, Huntsinger. China's grassland contract policy and its impacts on herder ability to benefit in Inner Mongolia: tragic feedbacks. *Ecology and Society.* 2011,16, 1-12.

49. Zhang F, Nilsson C, Xu Z, Zhou G. Evaluation of restoration approaches on the Inner Mongolian Steppe based on criteria of the Society for Ecological Restoration. *Land Degradation & Development.* 2020, 31, 285-296.

50. Chen K, Yang C, Bai L, Chen Y, Liu R, Chao L. Effects of natural and human factors on vegetation normalized difference vegetation index based on geographical detectors in Inner Mongolia. *Acta Ecol. Sin.* 2021, 41, 4963-4965.

51. Hao L, Sun G, Liu Y, Gao Z, He J, Shi T, Wu B. Effects of precipitation on grassland ecosystem restoration under grazing exclusion in Inner Mongolia, China. *Landscape Ecology*. 2014, 29, 1657-1673.

52. Xie B, Jia X, Qin Z, Shen J, Chang Q. Vegetation dynamics and climate change on the Loess Plateau, China: 1982–2011. *Regional Environmental Change*. 2016, 16, 1583-1594.

53. Hao J, Lin Q, Wu T, Chen J, Li W, Wu X, Hu G, La Y. Spatial–temporal and driving factors of land use/cover change in Mongolia from 1990 to 2021. Remote Sensing. 2023, 15, 1813.

54. Wang C, Wang S, Fu B, Lü Y, Liu Y, Wu X. Integrating vegetation suitability in sustainable revegetation for the Loess Plateau, China. Science of the Total Environment. 2021, 759, 143572.

55. Tong S, Zhang J, Bao Y, Lai Q, Lian X, Li N, Bao Y. Analyzing vegetation dynamic trend on the Mongolian

Plateau based on the Hurst exponent and influencing factors from 1982–2013. Journal of Geographical Sciences. 2018, 28, 595-610.

56. Su K, Liu H, Wang H. Spatial–temporal changes and driving force analysis of ecosystems in the Loess Plateau Ecological Screen. *Forests*. 2022, 13, 54.

57. Bromley J, Brouwer J, Barker AP, Gaze SR, Valentine C. The role of surface water redistribution in an area of patterned vegetation in a semi-arid environment, south-west Niger. *Journal of Hydrology*. 1997, 198, 1-29.

58. Yin H, Pflugmacher D, Li A, Li Z, Hostert P. Land use and land cover change in Inner Mongolia-understanding the effects of China's re-vegetation programs. *Remote Sensing of Environment*. 2018, 204, 918-930.

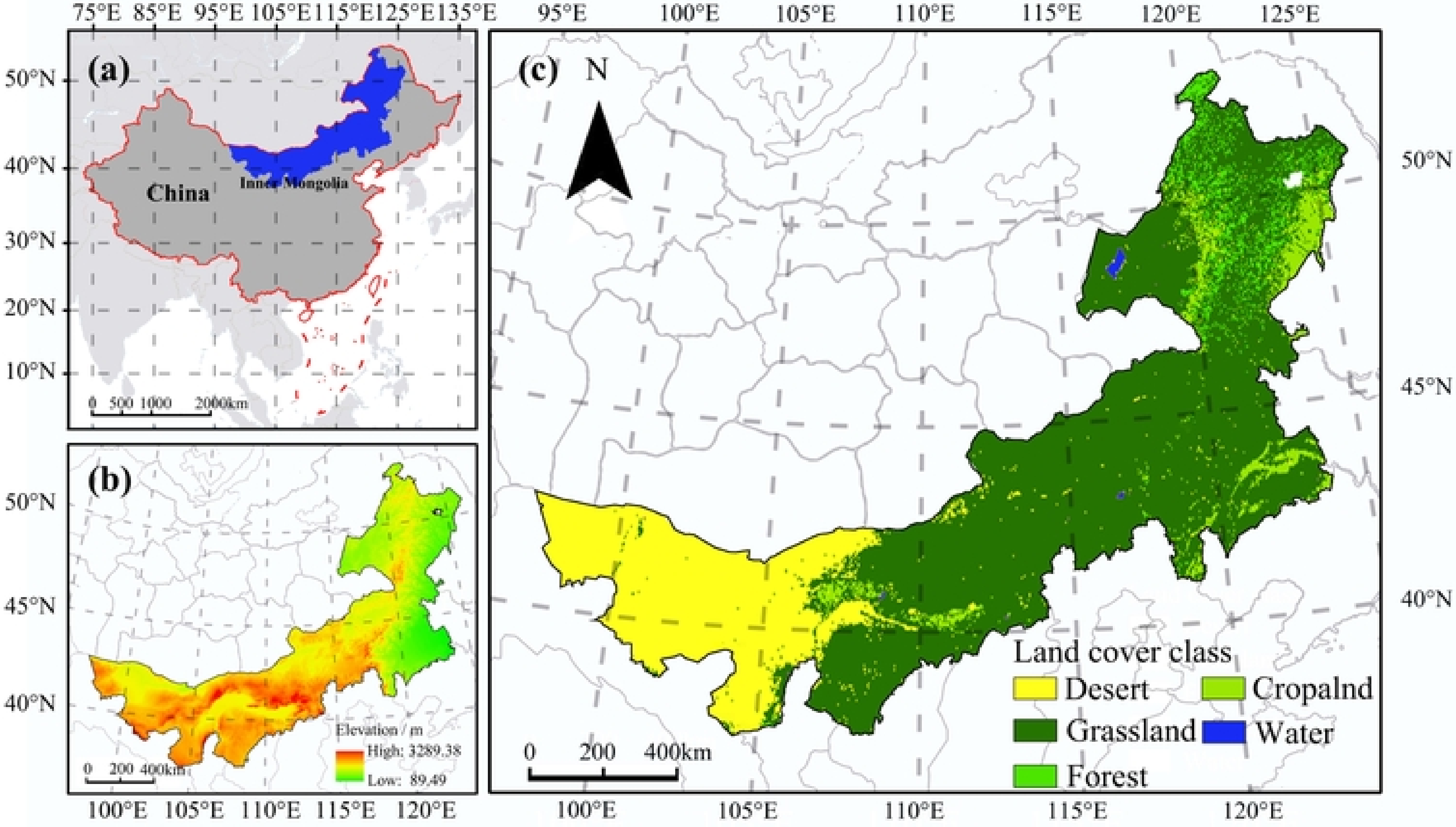

(a)
China
Inner Mongolia
75°E 85°E 95°E 105°E 115°E 125°E 135°E
50°N
40°N
30°N
20°N
10°N
0 500 1000 2000km
(b)
Elevation / m
High: 3289.38
Low: 89.49
0 200 400km
100°E 105°E 110°E 115°E 120°E
50°N
45°N
40°N
(c)
N
95°E 100°E 105°E 110°E 115°E 120°E 125°E
50°N
45°N
40°N
100°E 105°E 110°E 115°E 120°E
Land cover class
Desert
Cropalnd
Grassland
Water
Forest
0 200 400km

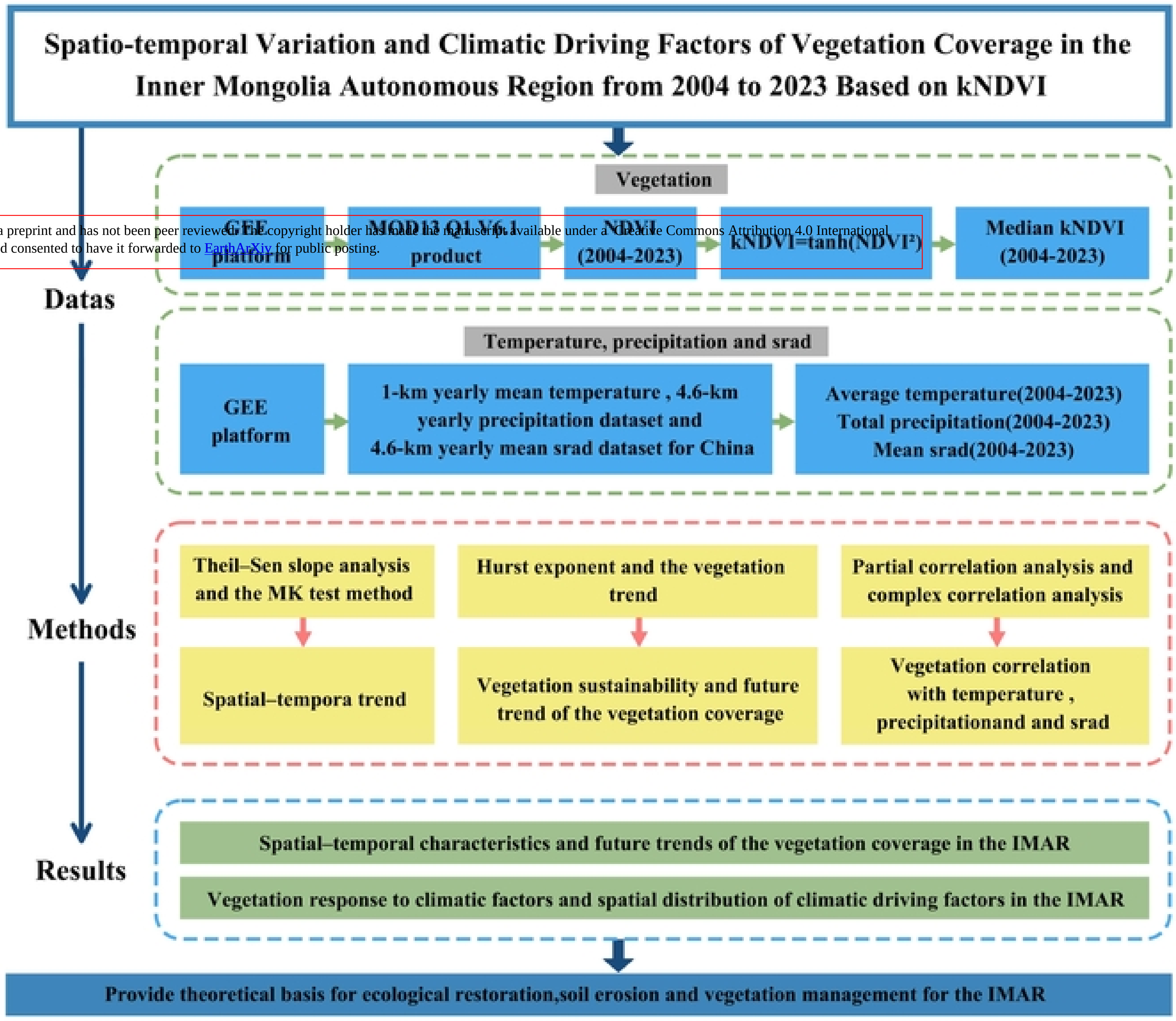
Spatio-temporal Variation and Climatic Driving Factors of Vegetation Coverage in the Inner Mongolia Autonomous Region from 2004 to 2023 Based on kNDVI
Vegetation
GEE platform
MOD13 Q1 V6.1 product
NDVI (2004-2023)
kNDVI=tanh(NDVI²)
Median kNDVI (2004-2023)
Datas
Temperature, precipitation and srad
GEE platform
1-km yearly mean temperature , 4.6-km yearly precipitation dataset and 4.6-km yearly mean srad dataset for China
Average temperature(2004-2023) Total precipitation(2004-2023) Mean srad(2004-2023)
Methods
Theil–Sen slope analysis and the MK test method
Hurst exponent and the vegetation trend
Partial correlation analysis and complex correlation analysis
Spatial–tempora trend
Vegetation sustainability and future trend of the vegetation coverage
Vegetation correlation with temperature , precipitationand and srad
Results
Spatial–temporal characteristics and future trends of the vegetation coverage in the IMAR
Vegetation response to climatic factors and spatial distribution of climatic driving factors in the IMAR
Provide theoretical basis for ecological restoration,soil erosion and vegetation management for the IMAR

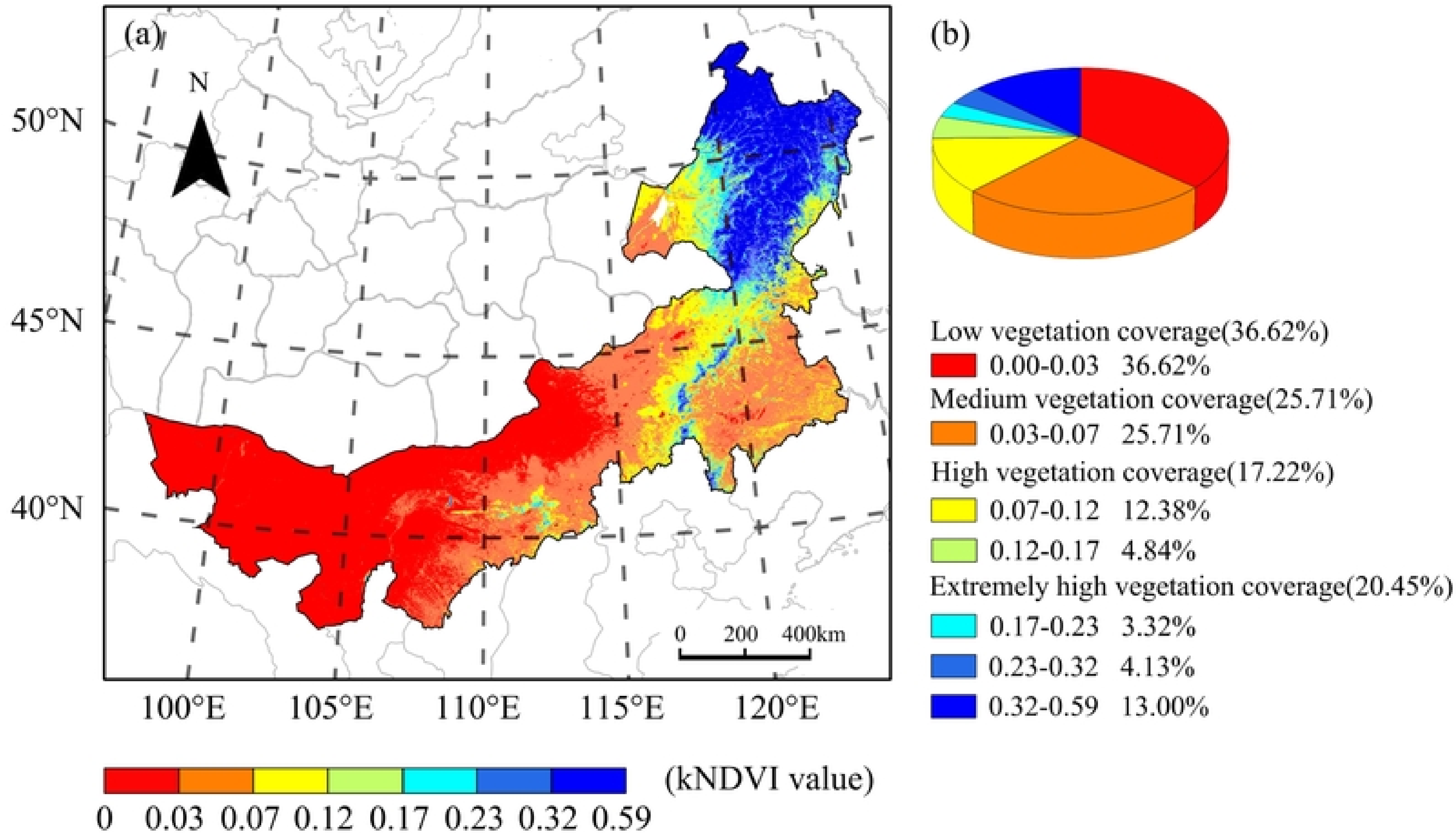
(a)
N
50°N
45°N
40°N
100°E
105°E
110°E
115°E
120°E
0 200 400km
(b)
Low vegetation coverage(36.62%)
0.00-0.03 36.62%
Medium vegetation coverage(25.71%)
0.03-0.07 25.71%
High vegetation coverage(17.22%)
0.07-0.12 12.38%
0.12-0.17 4.84%
Extremely high vegetation coverage(20.45%)
0.17-0.23 3.32%
0.23-0.32 4.13%
0.32-0.59 13.00%
(kNDVI value)
0 0.03 0.07 0.12 0.17 0.23 0.32 0.59

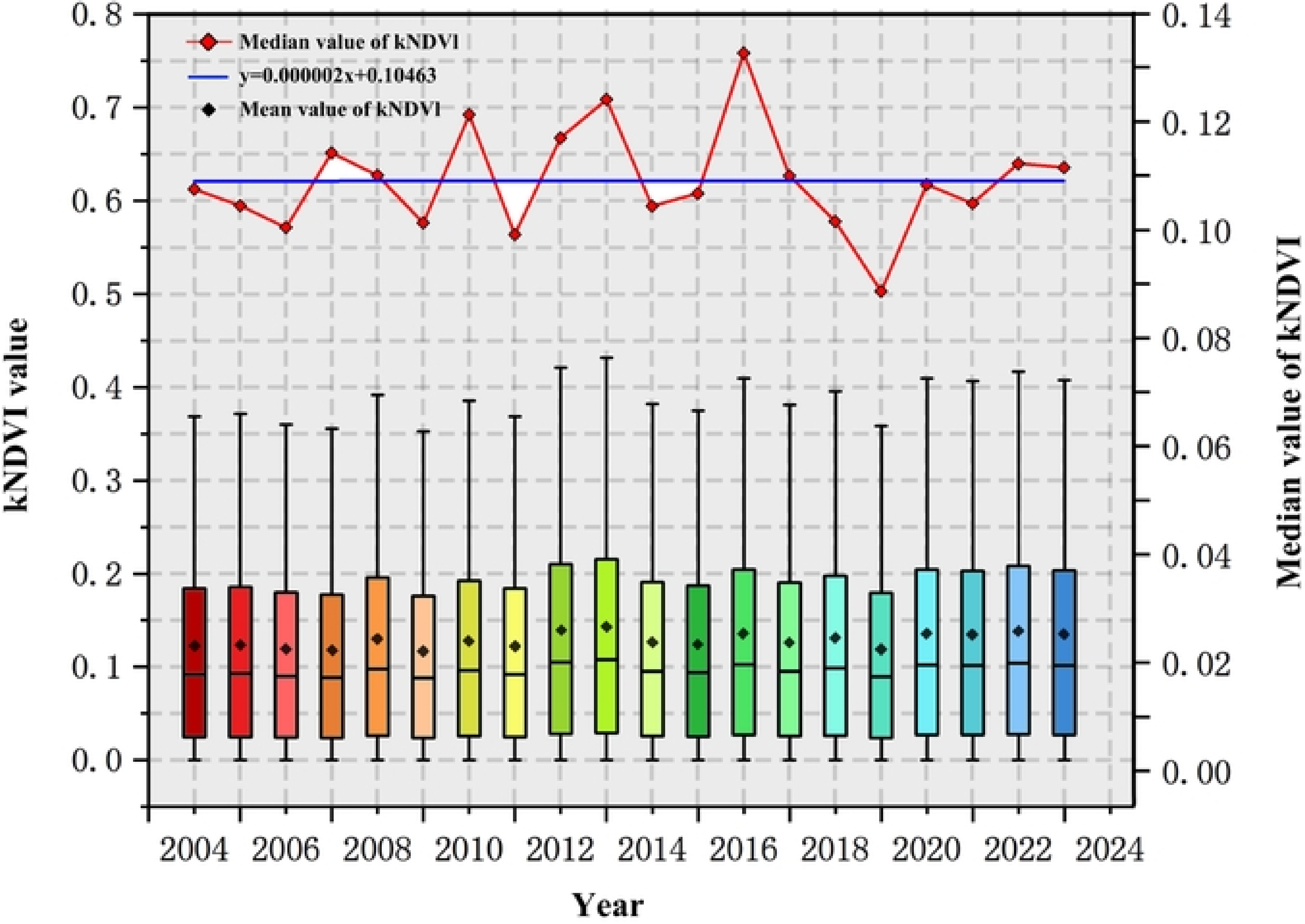
Median value of kNDVI
y=0.000002x+0.10463
Mean value of kNDVI
kNDVI value
Median value of kNDVI
Year
0.8
0.7
0.6
0.5
0.4
0.3
0.2
0.1
0.0
0.14
0.12
0.10
0.08
0.06
0.04
0.02
0.00
2004
2006
2008
2010
2012
2014
2016
2018
2020
2022
2024

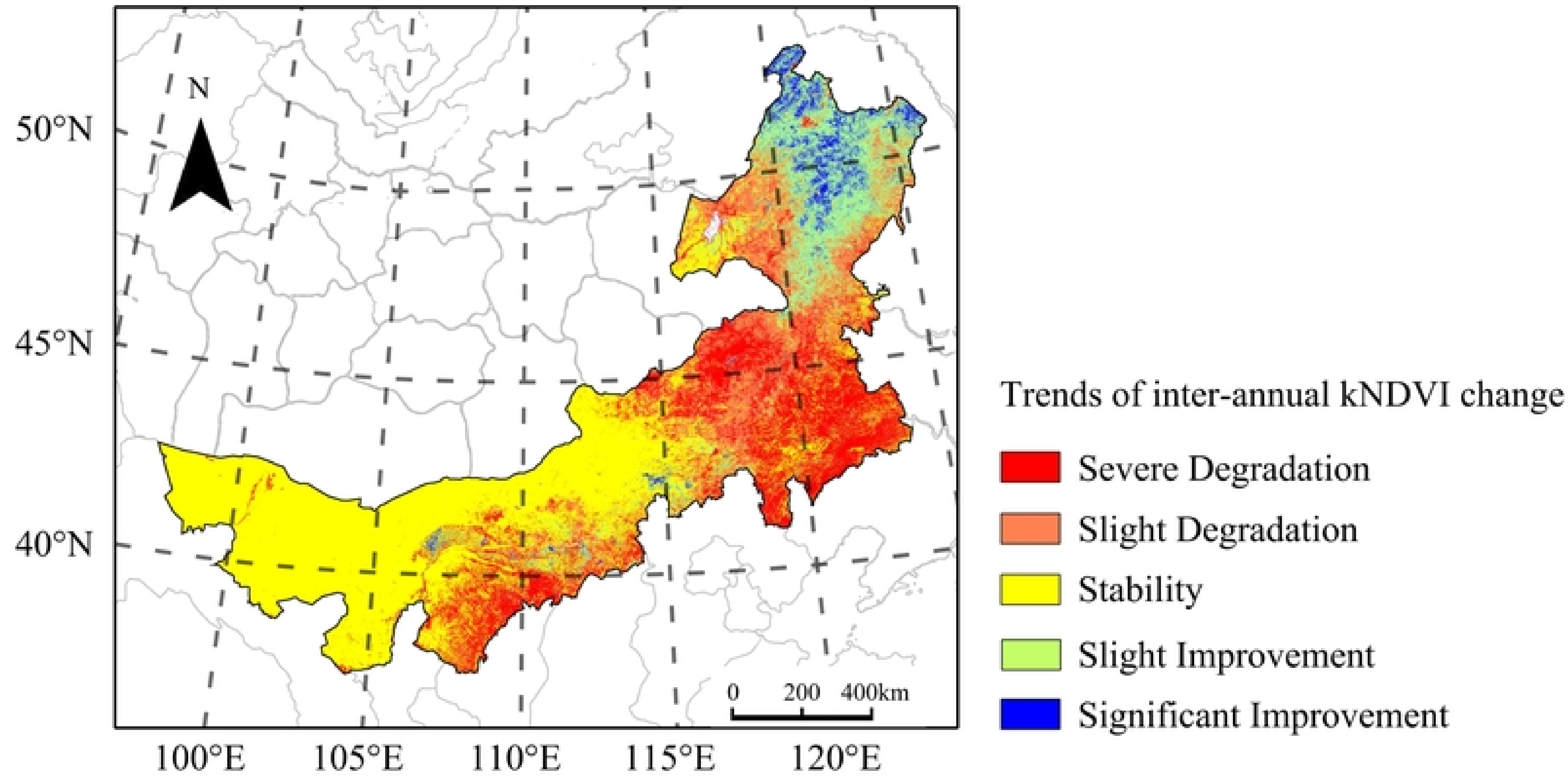
N
50°N
45°N
40°N
100°E
105°E
110°E
115°E
120°E
0
200
400km
Trends of inter-annual kNDVI change
Severe Degradation
Slight Degradation
Stability
Slight Improvement
Significant Improvement

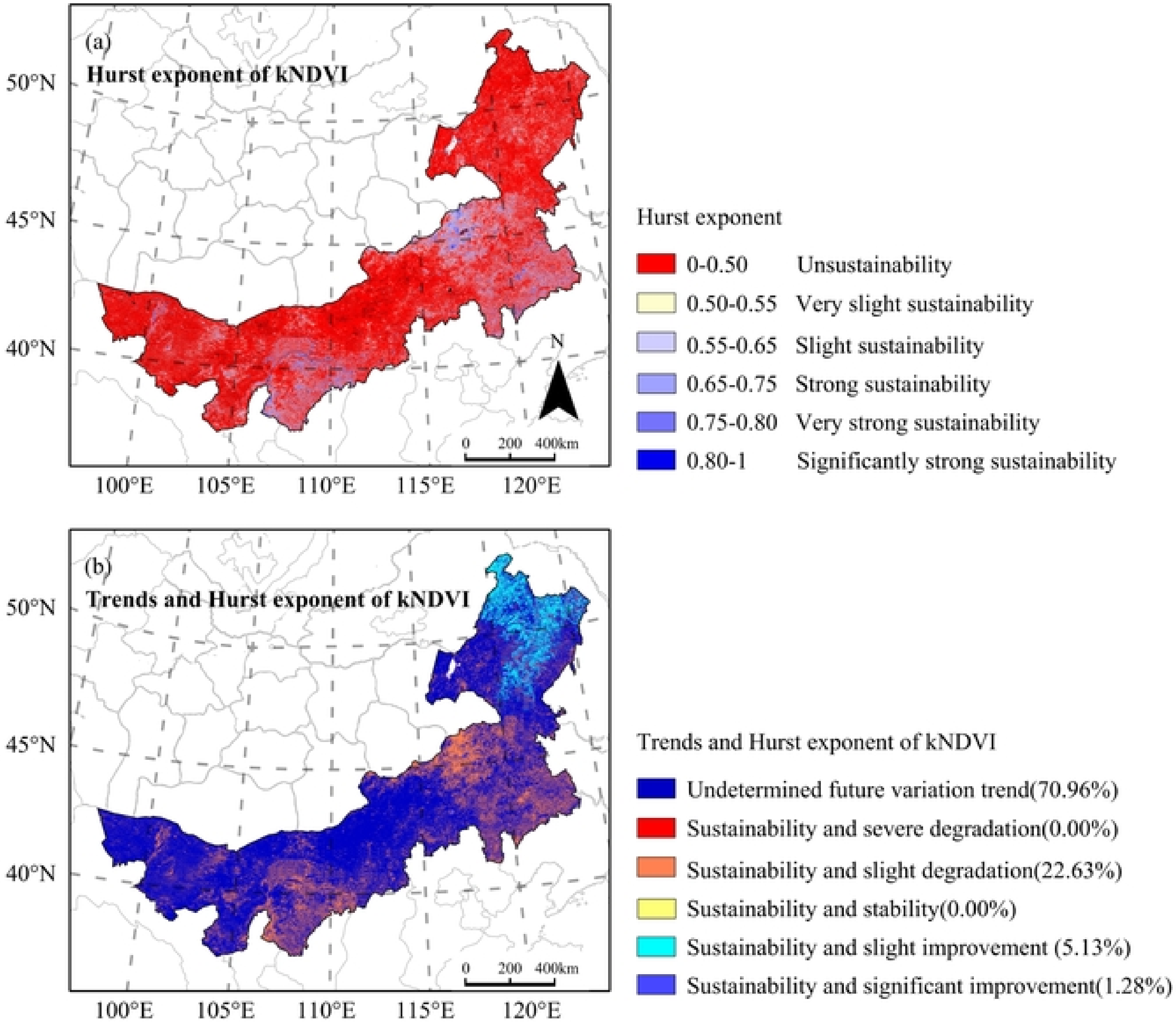
(a)
Hurst exponent of kNDVI
50°N
45°N
40°N
100°E
105°E
110°E
115°E
120°E
N
0
200
400km
Hurst exponent
0-0.50 Unsustainability
0.50-0.55 Very slight sustainability
0.55-0.65 Slight sustainability
0.65-0.75 Strong sustainability
0.75-0.80 Very strong sustainability
0.80-1 Significantly strong sustainability
(b)
Trends and Hurst exponent of kNDVI
50°N
45°N
40°N
100°E
105°E
110°E
115°E
120°E
0
200
400km
Trends and Hurst exponent of kNDVI
Undetermined future variation trend(70.96%)
Sustainability and severe degradation(0.00%)
Sustainability and slight degradation(22.63%)
Sustainability and stability(0.00%)
Sustainability and slight improvement (5.13%)
Sustainability and significant improvement(1.28%)

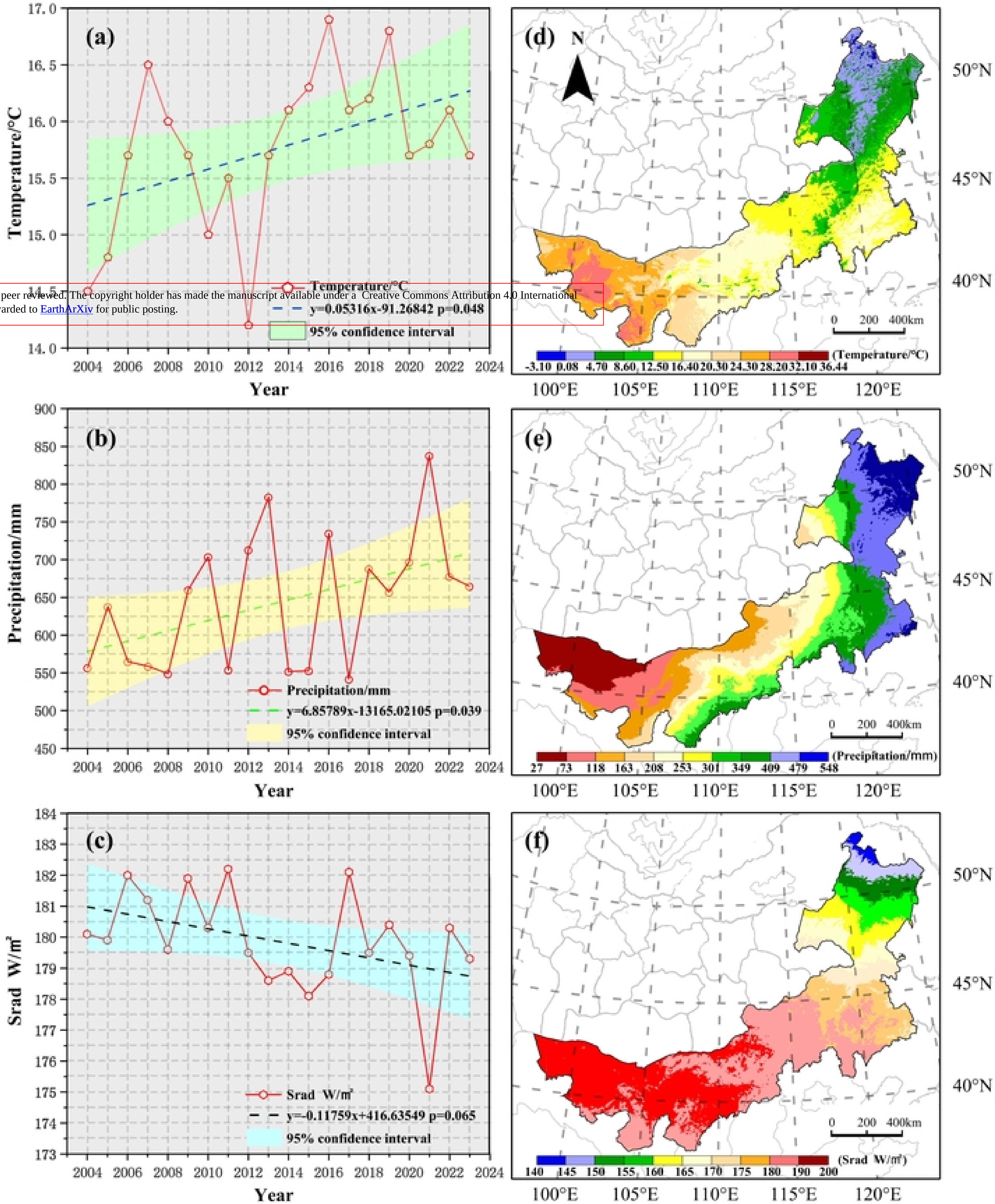
(a)
Temperature/°C
Year
Temperature/°C
y=0.05316x-91.26842 p=0.048
95% confidence interval
(b)
Precipitation/mm
Year
Precipitation/mm
y=6.85789x-13165.02105 p=0.039
95% confidence interval
(c)
Srad W/㎡
Year
Srad W/㎡
y=-0.11759x+416.63549 p=0.065
95% confidence interval
(d)
N
(Temperature/°C)
-3.10 0.08 4.70 8.60 12.50 16.40 20.30 24.30 28.20 32.10 36.44
(e)
(Precipitation/mm)
27 73 118 163 208 253 301 349 409 479 548
(f)
(Srad W/㎡)
140 145 150 155 160 165 170 175 180 190 200
0 200 400km
100°E 105°E 110°E 115°E 120°E
40°N 45°N 50°N

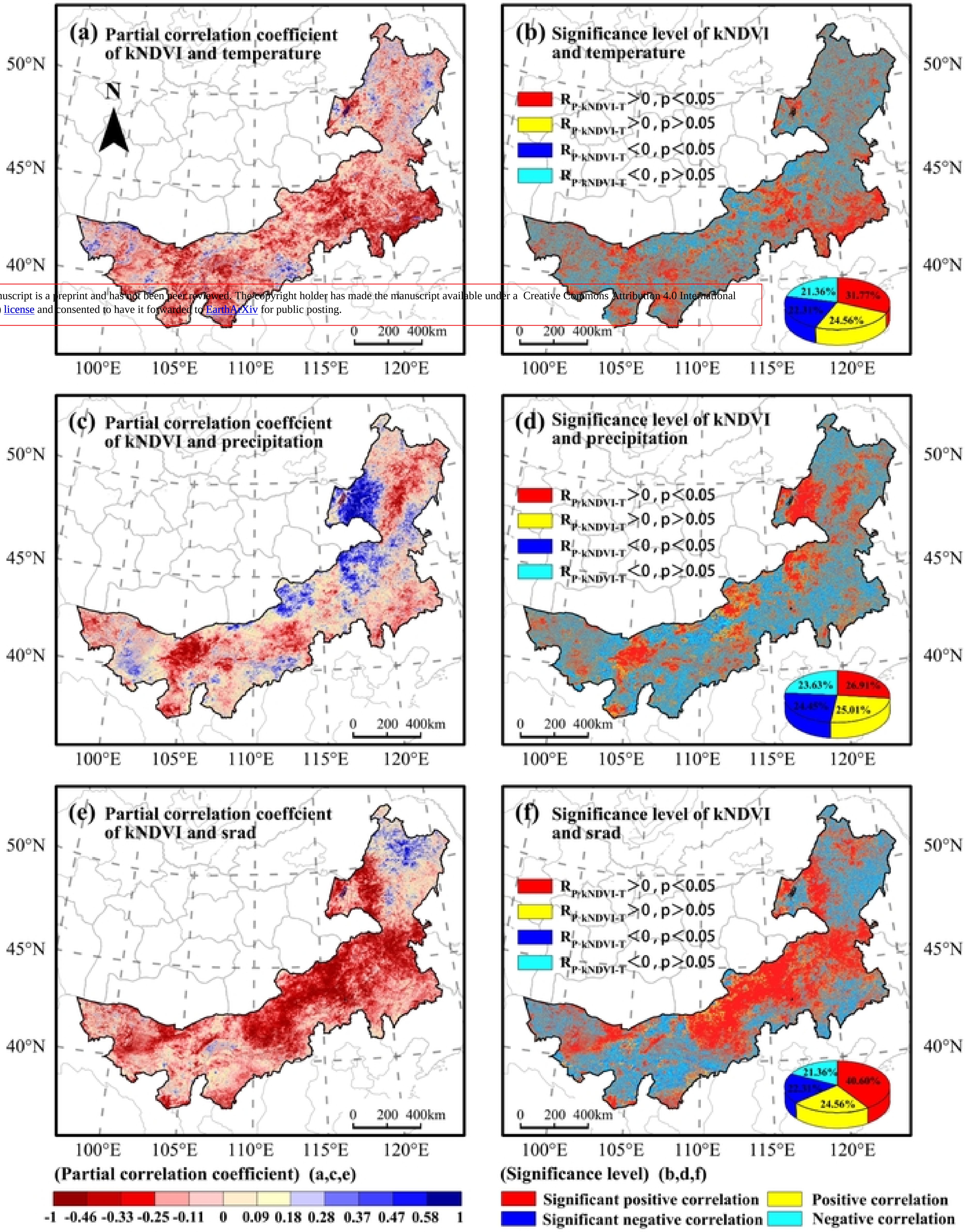
(a) Partial correlation coefficient of kNDVI and temperature
(b) Significance level of kNDVI and temperature
(c) Partial correlation coeffcient of kNDVI and precipitation
(d) Significance level of kNDVI and precipitation
(e) Partial correlation coeffcient of kNDVI and srad
(f) Significance level of kNDVI and srad
N
0 200 400km
50°N
45°N
40°N
100°E
105°E
110°E
115°E
120°E
R P-kNDVI-T >0 , p<0.05
R P-kNDVI-T >0 , p>0.05
R P-kNDVI-T <0 , p<0.05
R P-kNDVI-T <0 , p>0.05
21.36%
31.77%
24.56%
22.31%
23.63%
26.91%
24.45%
25.01%
40.60%
(Partial correlation coefficient) (a,c,e)
-1 -0.46 -0.33 -0.25 -0.11 0 0.09 0.18 0.28 0.37 0.47 0.58 1
(Significance level) (b,d,f)
Significant positive correlation
Positive correlation
Significant negative correlation
Negative correlation

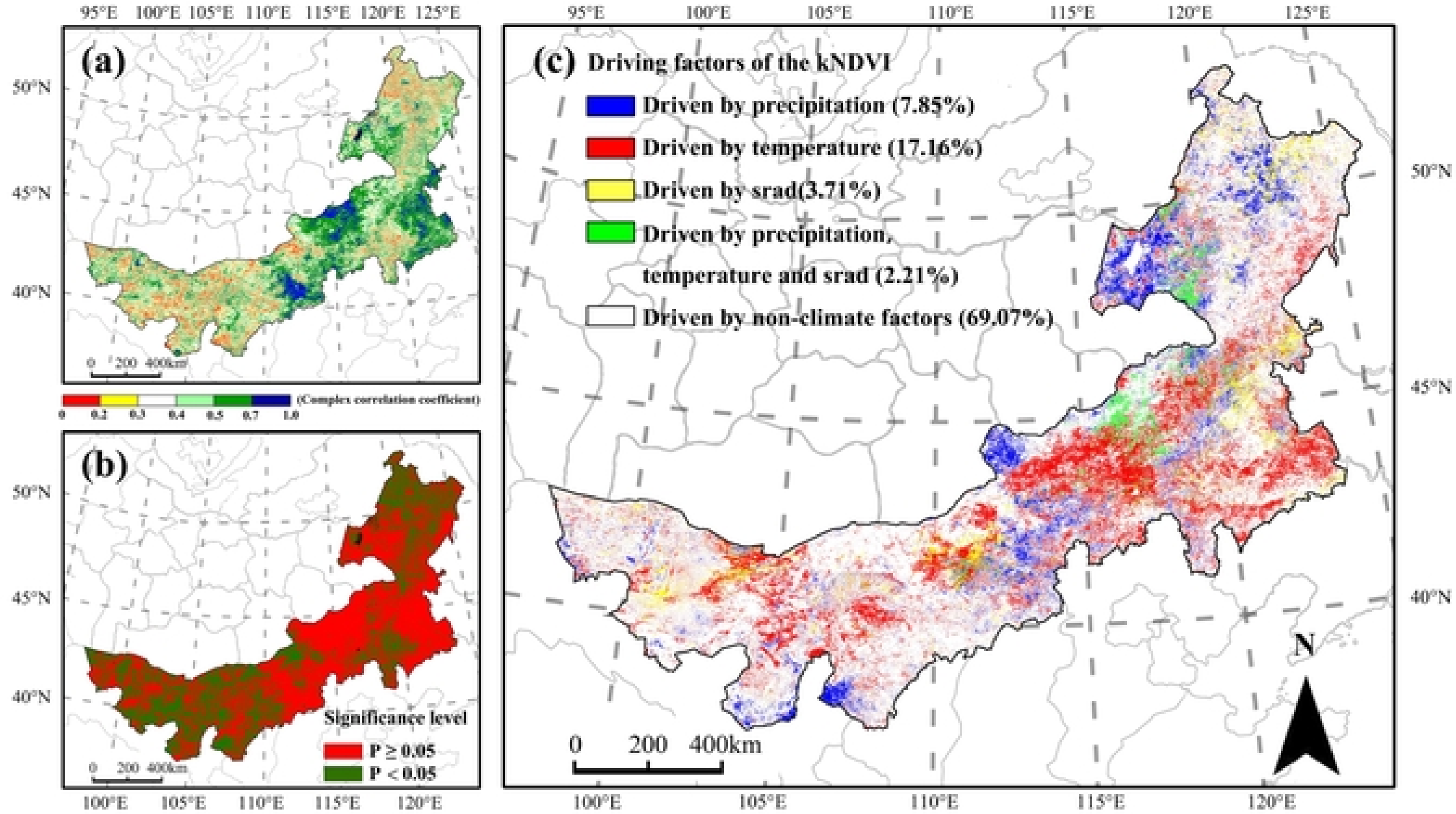
(a)
(b)
(c)
Driving factors of the kNDVI
Driven by precipitation (7.85%)
Driven by temperature (17.16%)
Driven by srad(3.71%)
Driven by precipitation, temperature and srad (2.21%)
Driven by non-climate factors (69.07%)
(Complex correlation coefficient)
0 0.2 0.3 0.4 0.5 0.7 1.0
Significance level
P ≥ 0.05
P < 0.05
0 200 400km
N
95°E 100°E 105°E 110°E 115°E 120°E 125°E
40°N 45°N 50°N

S_{KNDVI}	Z_s Value	kNDVI Trends	Area Percentage/%
≥0.0005	≥1.96	Significantly improved	18.90
≥0.0005	-1.96-1.96	Slightly improved	16.46
-0.0005—0.0005	-1.96-1.96	Stable	49.95
≤-0.0005	-1.96-1.96	Slightly degraded	11.38
≤-0.0005	≦-1.96	Severely degraded	3.31

Type of Driving Factor	Classification Basis			
	$R_{kNDVI-P}$	$R_{kNDVI-T}$	$R_{kNDVI-S}$	$R_{kNDVI-T-P-S}$
Driven by precipitation	$\|t\|>0.05$			$F>F_{0.05}$
Driven by temperature		$\|t\|>0.05$		$F>F_{0.05}$
Driven by srad			$\|t\|>0.05$	$F>F_{0.05}$
Driven by temperature precipitation and srad	$\|t\|<0.05$	$\|t\|<0.05$	$\|t\|<0.05$	$F>F_{0.05}$
Driven by non-climate factors				$F<F_{0.05}$